LANGMUIR

Article

pubs.acs.org/Langmuir

Aqueous Growth of Gold Clusters with Tunable Fluorescence Using Photochemically Modified Lipoic Acid-Based Ligands

Dinesh Mishra,[†] Fadi Aldeek,[†] Eric Lochner,[‡] Goutam Palui,[†] Birong Zeng,[†] Sebastian Mackowski,[§] and Hedi Mattoussi*[,†]

[†]Department of Chemistry and Biochemistry and [‡]CMMP, Department of Physics, Florida State University, Tallahassee, Florida 32306, United States

[§]Optics of Hybrid Nanostructures Group, Faculty of Physics, Astronomy and Informatics, Nicolaus Copernicus University, Grudziadzka 5/7, 87-100 Torun, Poland

Supporting Information

ABSTRACT: We report a one-phase aqueous growth of fluorescent gold nanoclusters (AuNCs) with tunable emission in the visible spectrum, using a ligand scaffold that is made of poly(ethylene glycol) segment appended with a metal coordinating lipoic acid at one end and a functional group at the other end. This synthetic scheme exploits the ability of the UV-induced photochemical transformation of LA-based ligands to provide DHLA and other thiol byproducts that exhibit great affinity to metal nanoparticles, obviating the need for chemical reduction of the dithiolane ring using classical reducing agents. The influence of various experimental conditions, including the photoirradiation time, gold precursor-to-ligand molar ratios, time of reaction, temperature, and the medium pH, on the growth of AuNCs has been systematically investigated. The photophysical properties, size, and structural characterization were carried out using UV−vis absorption and fluorescence spectroscopy, TEM, DOSY-NMR, and X-ray photoelectron spectroscopy. The hydrodynamic size (R_H) obtained by DOSY-NMR indicates that the size of these clusters follows the trend anticipated from the absorption and PL data, with R_H(red) > R_H(yellow) > R_H(blue). The tunable emission and size of these gold nanoclusters combined with their high biocompatibility would make them greatly promising for potential use in imaging and sensing applications.

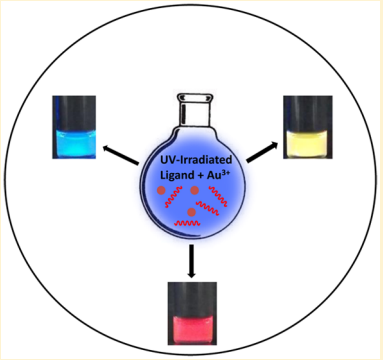

INTRODUCTION

Ultrasmall metallic nanoclusters (AuNCs) made of gold constitute a new class of nanomaterials with great potential for applications in catalysis as well as optical and electronic devices[1,2] and as fluorescent probes for biosensing.[3,4] They consist of a few to tens of atoms, and because their size is in a regime comparable to the Fermi wavelength of electrons, they can exhibit molecule-like properties, including size- and composition-dependent absorption and fluorescence.[5,6] Recent advances in the synthesis of inorganic nanomaterials have enabled the development of growth routes to prepare a variety of fluorescent nanocrystals with tunable emission over wide a range of the optical spectrum.[3,4,7−12] These materials are functionalized with ligands that play a crucial role in their colloidal stabilization and strongly influence their photophysical properties.

Growth methods to prepare AuNCs can be divided into two main ideas. The first is a top-down approach and involves the etching of larger size gold nanoparticles (AuNPs) into smaller fluorescent AuNCs, while the second, known as a bottom-up approach, involves the reduction of gold precursors, usually carried out in the presence of a chemical reagent.[7,13−17] However, noble metal clusters prepared using various chemical routes tend to vary from one approach to another in size, exact chemical structure, photophysical properties, and colloidal stability. The ligand structure, size, and coordination onto the metal atoms strongly affect the above properties, namely emission and solubility. In general, the fluorescence properties of these NCs are varied by controlling the nature of the capping ligand used during growth. Thus, a variety of ligands have been used in the growth of AuNCs, including thiol-containing oligomers,[15,18−21] dendrimers,[22,23] peptides,[24,25] proteins,[26,27] and polymers.[13,28] For example, Dickson and co-workers reported the use of PAMAM dendrimers to grow small, water-dispersible, and fluorescent AuNCs with discrete excitation and emission from a wide range of wavelengths; they further correlated the size of the clusters with the measured fluorescence emission.[23] They reported fluorescence quantum yields ranging from 10 to 70% for these materials. Jin and co-workers extensively reported on the growth and characterization of Au clusters,[29−31] and in a recent study they showed that growing 25-atom Au/Ag bimetallic clusters by mixing triphenylphosphine-capped Au_{11} clusters with silver(I)−thiolate complexes could yield materials that emit around 670 nm with high PL efficiency and well-defined optical properties.[30] An increase of ∼200-fold emission has been measured

Received: March 18, 2016
Revised: May 19, 2016
Published: June 2, 2016

DOI: 10.1021/acs.langmuir.6b00950
Langmuir 2016, 32, 6445−6458

compared to the poorly emitting initial Au clusters. Xie and co-workers have also reported several schemes for growing gold clusters.[32−35] In particular, they showed, in a recent study, that growing clusters with precise mass ($Au_{22}(SR)_{18}$) capped with long thiolate ligands yielded red-emitting materials (with a peak at ∼665 nm and a QY of ∼8%), whereas clusters prepared with 17 and 25 Au atoms were not emitting.[32] Their study showed that the aggregation of Au(I) motifs on the cluster surface is the driving factor for high fluorescence in these clusters. In earlier work Xie, Ying, and co-workers reported the preparation of red-emitting AuNCs with high quantum yield by relying on the "biomineralization" capability of bovine serum albumin (BSA) and using a one-pot growth route.[33] Pradeep and co-workers reported the growth of red-emitting AuNCs (emission peak at ∼640−650 nm) using an iron binding transferrin protein, lactoferrin.[27] Blue-emitting AuNCs were also prepared using citrate reduction of Au precursors in the presence of polycytosine DNAs in acidic pH or in the presence of polyadenine at neutral pH.[36] Integration of luminescent metal clusters, namely those made of Au cores into biological applications, has also been pursued by a few groups.[14,37−39] Zheng and co-workers have grown thiolated PEG- or zwitterion-stabilized luminescent gold nanoparticles and tested their clearance and tumor targeting depending on whether PEG or ZW coating was used. They found that PEG coating increases the blood circulation, thus enhancing the degree of tumor targeting in live mice.[39]

Over the past few years, our group has developed several multifunctional metal-coordinating ligands and applied them to the surface functionalization of semiconductor quantum dots and metal nanoparticles.[40−42] These ligands are made of a single or multiple lipoic acid, LA (or dihydrolipoic acid, DHLA), groups that can strongly coordinate onto the inorganic surfaces of the nanocrystals, combined with tunable length poly(ethylene glycol) or zwitterion segments to promote hydrophilicity. The use of LA-based ligands (PEGylated or zwitterion) to cap fluorescent NPs drastically reduces non-specific interactions and aggregation of the NPs in biological media. The LA-PEG ligands can be further functionalized with bioreactive groups such as amine and carboxyl groups to promote bioconjugation of the NPs to target molecules. In 2010, we reported the use of these LA-PEG ligands to grow, via a one-phase aqueous growth method, AuNPs with sizes ranging from 2 to 20 nm.[41] The control over size was achieved by varying the molar ratios between the gold precursor and ligands used in the reaction. Molar ratios of Au-to-ligand greater than 1 led to the formation of AuNPs larger than 2 nm in diameter, whereas ratios smaller than 1 yielded AuNPs that are smaller than 2 nm. Furthermore, this growth route provided AuNPs that exhibit great colloidal stability over a broad range of conditions. This strategy was subsequently expanded to grow silver and gold NPs using both LA-PEG and LA-zwitterion ligands, where under specific conditions of high ligand-to-metal-precursor molar ratios and basic conditions fluorescent silver and gold NCs with red and NIR fluorescence emission (680 nm for AgNCs and 740 nm for AuNCs) can be prepared.[43,44] A common feature of the aforementioned growth route is the formation of an Au(I)−thiolate precursor followed by reduction using sodium borohydride, which is known to drive the reduction of Au(I) ion to metallic gold Au(0).[11,45]

In separate studies, we have reported that reduction of lipoic acid (LA) to dihydrolipoic acid (DHLA), which is a prerequisite for the surface functionalization of luminescent ZnS-overcoated QDs, can be carried out chemically using $NaBH_4$.[42,46] Although $NaBH_4$ reduction has been effective for preparing DHLA-PEG ligands, it tends to alter the chemical composition of some functional groups (such as azide and aldehyde) and further requires additional processing and stringent inert storage conditions. Recently, we have demonstrated that if the photosensitive nature of the dithiolane ring were taken into consideration, UV-irradiation of a dispersion of hydrophobic CdSe−ZnS QDs mixed with the oxidized form of the ligands would promote *in situ* ligand exchange and phase transfer of the QDs to buffer media.[47] Indeed, this photoligation strategy has provided high quality hydrophilic nanocrystals, while preserving the photophysical properties of the QDs and the integrity of sensitive functional groups.[47,48] We have also found that photoirradiation of the lipoic acid generates several byproducts, including thiol radicals, monomeric dihydrolipoic acid, and oligomers.[48]

Here, we build on those developments and report the use of photochemically modified LA-PEG ligands, combined with a one-pot aqueous growth, to prepare fluorescent AuNCs with tunable properties. The reaction is borohydride-free and relies on the photochemical modification of LA-PEG ligand prior to mixing with the Au precursors. The lipoic acid-based ligand is first irradiated with UV signal at 350 nm and then mixed with gold chloride precursor, followed by growth under refluxing conditions (at 100 °C). This route yields Au clusters that exhibit broad optical excitation with tunable photoluminescence and great long-term colloidal stability under several biologically relevant conditions.

EXPERIMENTAL SECTION

Reagents. Chloroauric acid trihydrate, $HAuCl_4{\cdot}3H_2O$ (99.9%), (±)-α-lipoic acid, poly(ethylene glycol) (MW ≈ 600 g/mol), poly(ethylene glycol) methyl ether (MW ≈ 750 g/mol), methanesulfonyl chloride (99.7%), triphenylphosphine, TPP (99%), 4-(*N*,*N*-dimethylamino)pyridine (99%), triethylamine (Et_3N), *N*,*N*-dicyclohexylcarbodiimide, sodium borohydride ($NaBH_4$), succinic anyhydride, 1-ethyl-3-(3-(dimethylamino)propyl)carbodiimide hydrochloride, *N*-hydroxysuccinimide NHS (98%), NaOH, KOH, $NaHCO_3$, organic solvents (THF, $CHCl_3$, etc.), salts (such as NaCl and Na_2SO_4), and Rhodamine 6G were purchased from Sigma Chemicals (St. Louis, MO). Sodium azide (99%), *N*,*N*-dimethyl-1,3-propanediamine (99%), and 1,3-propane sultone (99%) were purchased from Alfa-Aesar (Ward Hill, MA). The reagents were used as purchased unless otherwise specified. Column purification chromatography was performed using silica gel (60 Å, 230−400 mesh, purchased from Bodman Industries (Aston, PA)). PD10 columns for size exclusion chromatography were purchased from GE Healthcare (Piscataway, NJ).

Instrumentation, Data Collection, and Analyses. Photoirradiation of the ligands was carried out using a photoreactor from Luzchem Research, Inc. (Model LZC-4 V, Ottawa, Canada). The UV−vis absorption measurements were carried out using a UV 2450 absorption spectrophotometer from Shimadzu (Columbia, MD), while the fluorescence emission and excitation spectra were collected using a Fluorolog-3 spectrometer equipped with CCD and PMT detectors from Horiba Jobin Yvon Inc. (Edison, NJ). The fluorescence lifetime measurements were carried out using a time correlation single photon counting (TCSPC) system integrated into the same Fluorolog-3. We used a pulsed excitation signal at 440 nm with a repetition rate of 1 MHz, provided by NanoLED-440LH (100 ps, fwhm), while emission was collected with the same PMT detector as above. The fluorescence decay traces of the AuNCs emission (limited to a narrow window centered at the peak of the PL spectrum) were analyzed using the TCSPC system and fitted to a three-exponential function of the form

DOI: 10.1021/acs.langmuir.6b00950
Langmuir 2016, 32, 6445−6458

$$I(t) = A_1 e^{-t/\tau_1} + A_2 e^{-t/\tau_2} + A_3 e^{-t/\tau_3} \quad (1)$$

where t is time and A_i is a weighting parameter associated with each decay time, τ_i. We then used this fit to extract an average amplitude-weighted lifetime, τ_{avg}, as

$$\tau_{avg} = \frac{\sum A_i \tau_i^2}{\sum A_i \tau_i} \quad (2)$$

The fluorescence quantum yield (QY) of the AuNCs was extracted from experimental data (compared to standard materials) using the equation

$$QY_{sample} = \frac{F_{sample}}{F_{ref}} \times \frac{A_{ref}}{A_{sample}} \times \frac{n_{sample}^2}{n_{ref}^2} \times QY_{ref} \quad (3)$$

where F, A, and n are the measured fluorescence intensity (integrated area under the emission peak), the absorbance at the excitation wavelength, and the refractive index of the solvent, respectively. As reference fluorophores we used Rhodamine 6G (QY_{ref} = 95% in ethanol) and 4,6-diamidino-2-phenylindole (DAPI) (QY_{ref} = 4%). The TEM images were collected using a JEOL-2010 200 kV instrument. Samples for transmission electron microscopy (TEM) were prepared by drop-casting the AuNC dispersions onto a holey carbon film on a fine-mesh Cu grid (400 mesh) and letting it dry.

X-ray Photoelectron Spectroscopy (XPS). XPS measurements were carried out using a PHI 5000 series instrument from PHI Inc. (Chanhassen, MN) equipped with a monochromated Al Kα source (1486.7 eV), and the pass energy of the analyzer was maintained at 89.45 eV. The photoelectron takeoff angle was 45° relative to the sample surface. The binding energy (BE) scale of the system was calibrated using Au $4f_{7/2}$ = 83.8 eV and Cu $2p_{3/2}$ = 932.67 eV, which was sputtered clean using Ar^+, typically at 3 kV to ensure that any chemically modified adlayers have been removed. The base pressure of the UHV analysis chamber was 6×10^{-10} mbar. A Shirley background was subtracted from all spectra before peak fitting with a Gaussian–Lorentzian function was performed.

Diffusion-Ordered NMR Spectroscopy (DOSY) Measurements. DOSY NMR spectra were collected using a Bruker SpectroSpin 600 MHz spectrometer (Bellerica, MA). The spectra were acquired using LED-bipolar gradient pulse sequence (ledbpgp2s) with 32K and 32 points in t_2 and t_1, respectively, and each 2D slice represents the signal averaged over 32 scans. The typical experimental parameters for collecting a DOSY spectrum were as follows: acquisition time 2.0 s, gradient strength G 45 G/cm, diffusion delay time 300 ms, gradient duration 1.8 ms, and relaxation delay 5.0 s. The diffusion time was optimized for every experiment, and the diffusion coefficient was generally achieved by stepwise ramping up the amplitudes of pulsed field gradients. Reference deconvolution and baseline correction were adopted to compensate for experimental imperfections.[49]

Synthesis of the LA-PEG Ligands. Three sets of ligands made of a lipoic acid appended with poly(ethylene glycol) terminated with either methyl ether (inert), or a reactive functional group, used for the growth and functionalization of the AuNCs, have been synthesized following previously reported protocols: LA-PEG_{750}-OCH_3 (PEG MW = 750), LA-PEG_{600}-COOH (PEG MW = 600), and LA-PEG_{600}-NH_2 (PEG MW = 600).[50,51] Briefly, to prepare LA-PEG-OCH_3, the terminal hydroxyl group of poly(ethylene glycol) methyl ether was transformed into azide. Then, the azide was converted to amine using triphenylphosphine, followed by attachment to lipoic acid (LA) through DCC coupling to provide the final LA-PEG-OCH_3. Similarly, LA-PEG-NH_2 and LA-PEG-COOH were prepared starting from poly(ethylene glycol). Both terminal hydroxyl groups were transformed to azides, followed by a selective conversion of one azide to an amine and then attachment to lipoic acid to provide LA-PEG-N_3. The latter was further transformed to LA-PEG-NH_2 using triphenylphosphine; LA-PEG-COOH was prepared by transforming the amine group of LA-PEG-NH_2 in the presence of succinic anhydride.

Growth of Red-, Yellow-, and Blue-Emitting AuNCs. A solution of LA-PEG ligand (terminating in $-OCH_3$, $-NH_2$, or $-COOH$) in DI water (1.6 mL, 15 mM concentration) was prepared in a scintillation vial. The vial was placed inside a UV photoreactor and irradiated with signal at 350 nm for 40 min while stirring. To the solution of irradiated ligands, 80 μL of $HAuCl_4 \cdot 3H_2O$ stock solution (50 mM) was added along with DI water to bring the final volume of the reaction to 8 mL and the molar ratio of gold precursor-to-ligand to 1-to-6. Then, 40 μL of 2 M aqueous NaOH solution was added to make the reaction mixture basic (at pH 11). The mixture was then immersed in an oil bath at 100 °C and left stirring. (Other growth temperatures ranging between ambient conditions and 100 °C were also explored.) Using these growth conditions yielded yellow-emitting NCs after 2 h, but when the mixture was left stirring at 100 °C overnight, red- or blue-emitting NCs were prepared depending on the exact structure of the ligand used. In particular, red-emitting clusters were obtained with a LA-PEG-OCH_3 ligand and blue-emitting clusters were formed when LA-PEG-NH_2 was used during the overnight growth. The red-emitting NCs were purified by applying 3–4 cycles of centrifugation/dilution using a membrane filtration device (Amicon Ultra with cutoff MW = 10 kDa, Millipore); these clusters did not pass through the membrane filter. In contrast, yellow-emitting clusters could not be purified using this device because they passed through the membrane filter; they were smaller than the cutoff MW of the device. To circumvent this constraint, the yellow-emitting clusters were first extracted in chloroform after the growth was stopped. The resulting solution had a bright green emission (when excited at 350 nm using a hand-held UV lamp), with a spectrum centered at 500 nm (see below). After evaporating the chloroform under vacuum, the clusters were readily dispersible in water with a bright yellow emission. This dispersion was purified using a PD10 column to remove excess free ligands. To purify the blue-emitting clusters, the brown growth solution was first filtered using a membrane filtration device (10 kDa cutoff MW), and the clean filtrate was collected and passed through a PD10 column to remove the excess free ligand. The resulting dispersions were stored at 4 °C until further use.

Colloidal Stability Tests. Following growth and purification aliquots from a concentrated stock solution of the NCs were transferred into Eppendorf tubes and lyophilized. The dried clusters were dispersed in 50 mM PBS buffers at different pH to a total volume of 300 μL; the same procedure was applied for each set of clusters. This yielded several dispersions of red-, yellow-, and blue-emitting clusters at pH ranging from pH 2 to pH 12. The dispersions were stored at 4 °C and then regularly retrieved and inspected for signs of aggregation buildup, and the fluorescence was visually checked under UV lamp. All samples were tracked for several months of storage following preparation and purification.

RESULTS AND DISCUSSION

Motivation and Rationale. The present strategy to grow clusters capped with LA-PEG ligands that exhibit tunable emission has been inspired by two recent seemingly independent developments. (1) The ability of the one phase aqueous growth, via borohydride reduction, to make LA-PEG- and LA-zwitterion-stabilized AuNPs and AgNPs with good size control in the range 1.5–18 nm in diameter, achieved by varying the gold precursor-to-ligand molar ratio.[41] In the presence of excess ligands (i.e., ligands are mixed with Au precursor in molar excess), the above route also provided fluorescent gold and silver NCs that emit in the far red with relatively high quantum yields.[43,44] (2) The ability of the UV-induced photochemical transformation of LA-based ligands to provide DHLA and other thiol derivatives that exhibit great affinity to the metal-rich surfaces of CdSe–ZnS QDs, obviating the need for chemical reduction of the dithiolane ring using $NaBH_4$. Indeed, lipoic acid (LA) has a well-defined absorption peak around 335 nm due to the presence of a strained five-

DOI: 10.1021/acs.langmuir.6b00950
Langmuir 2016, 32, 6445–6458

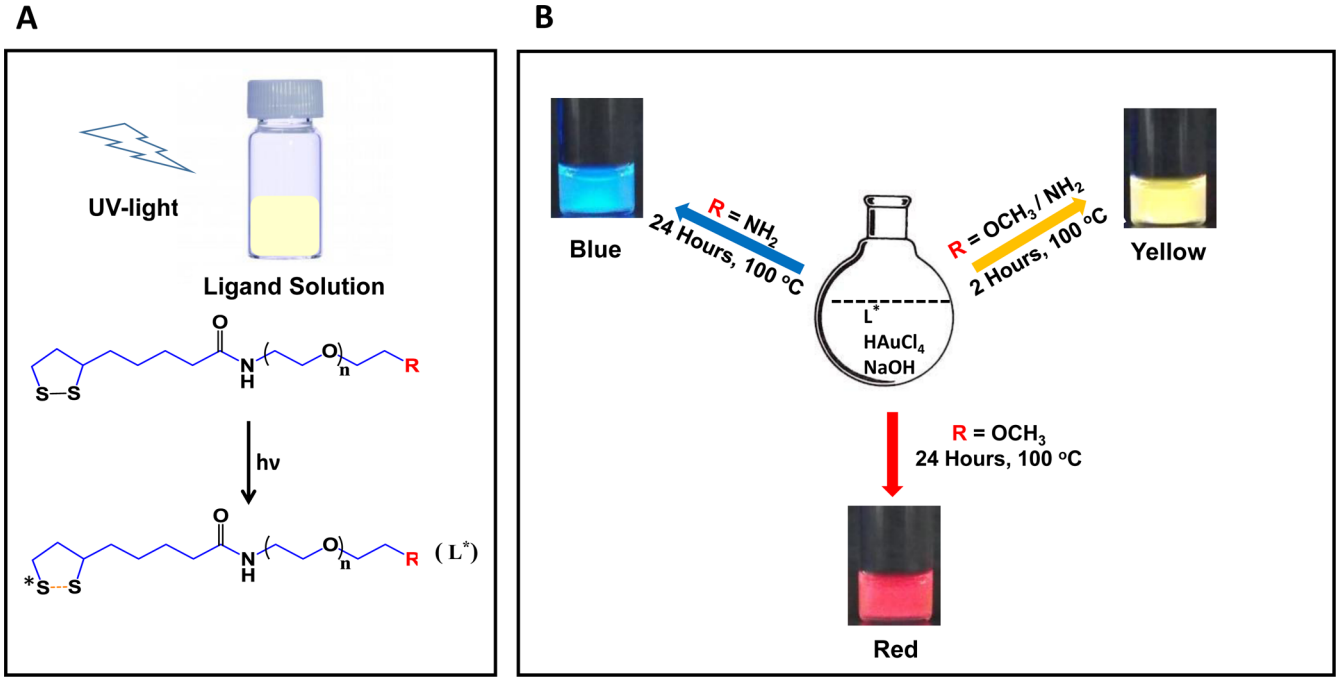

Figure 1. Schematic representation of the cluster growth strategy. (A) Ligand irradiation under UV light (350 nm). (B) An illustration of the growth of AuNCs with tunable emission.

membered trimethylene disulfide ring. The latter can be photochemically transformed by UV-irradiation. For instance, several studies have shown that irradiation of lipoic acid at 330−350 nm produces an excited singlet, which may result in either homolytic cleavage of the S−S or C−S bond, or intersystem crossing (ISC) to the triplet state.[47,52] Three pathways were proposed for the decay of the diradical resulting from homolytic cleavage of the S−S bond: ring closure leading back to the precursor lipoic acid, 1,4-H shift giving mercapto-thioaldehyde derivative, or 1,2-H shift giving mercaptoalkyl thiyl radical. Another possible pathway involves oligomer formation promoted by sulfur-to-sulfur bridging, initiated by photolysis of 1,2-dithiolane in neutral solution.

Here, we reasoned that combining these two developments and starting with UV-irradiated LA-PEG ligand mixed with chloroauric acid ($HAuCl_4{\cdot}3H_2O$) as precursor materials, Au nanoclusters with different properties can be prepared under borohydride-free conditions. We anticipated that by avoiding the use of a strong reducing agent, the growth kinetics can be slowed down, leading to the formation of clusters with tunable optical absorption and emission. In addition, the combination of high binding affinity of thiol to gold with the hydrophilic nature of PEG should provide effective stabilization of the AuNCs. Figure 1 shows a schematic diagram of the growth scheme employed here using photoirradiated LA-PEG ligands under basic conditions. At first, a solution of the ligand is irradiated (at 350 nm) using a UV photoreactor, which leads to a photochemical transformation of the LA group ($L + h\nu \rightarrow L^*$). When this solution is mixed with $HAuCl_4{\cdot}3H_2O$, using large excess ligands (Au:L* = 1:3−1:6), gold(III) complexes with L*. Such complexation is expected to be different in nature from the one already documented when mixing LA-PEG-OCH_3 with $HAuCl_4{\cdot}3H_2O$.[41] By controlling a series of parameters, including pH, temperature, ligand irradiation time, and reagent concentrations, AuNCs with distinct emissions can be prepared and characterized. In the following we will detail the optimized conditions developed to grow three sets of clusters with red, yellow, and blue fluorescence emission.

Optimization of the Growth Conditions. In order to identify the optimal reaction conditions, we first characterized the photoinduced chemical transformation of the ligands in water solution; this is important as the growth is carried out in aqueous media. It has been shown that the absorption spectrum of LA-PEG-OCH_3 displays a well-defined absorption peak around 335 nm, ascribed to the dithiolane ring, and under UV irradiation at 350 nm in organic solutions that peak progressively diminishes with increasing irradiation time and eventually disappears after 20−30 min.[47] We monitored changes in the absorption spectrum with increasing irradiation time of LA-PEG-OCH_3 in water and found that there was a net decrease in the absorbance at 335 nm with increasing irradiation time, with saturation reached after 30−40 min. Furthermore, the absorption spectrum at saturation did not reach background values as was the case when UV irradiation was carried out in methanol or chloroform (see Supporting Information, Figure S1).[47]

We then identified the key parameters that control the growth reaction from few preliminary experiments. These experiments suggested that UV irradiation of the ligand, alkaline pH of the medium, and elevated temperature promote the growth of AuNCs with clear fluorescence signal. The conditions of the reactions identified from those preliminary tests are summarized in the Supporting Information (Figure S2), where an image of vials containing particular reaction mixtures are visualized under UV illumination using a hand-held lamp. Once the broadly defined conditions were identified, we then thoroughly investigated the role of each parameter in greater details. Below, we describe the effects of those parameters on the overall growth of the AuNCs.

Effects of pH and Temperature. We tested the effects of varying the pH of the reaction from 8 to 11 and temperature from 25 °C (room temperature) to 100 °C (refluxing

DOI: 10.1021/acs.langmuir.6b00950
Langmuir 2016, 32, 6445−6458

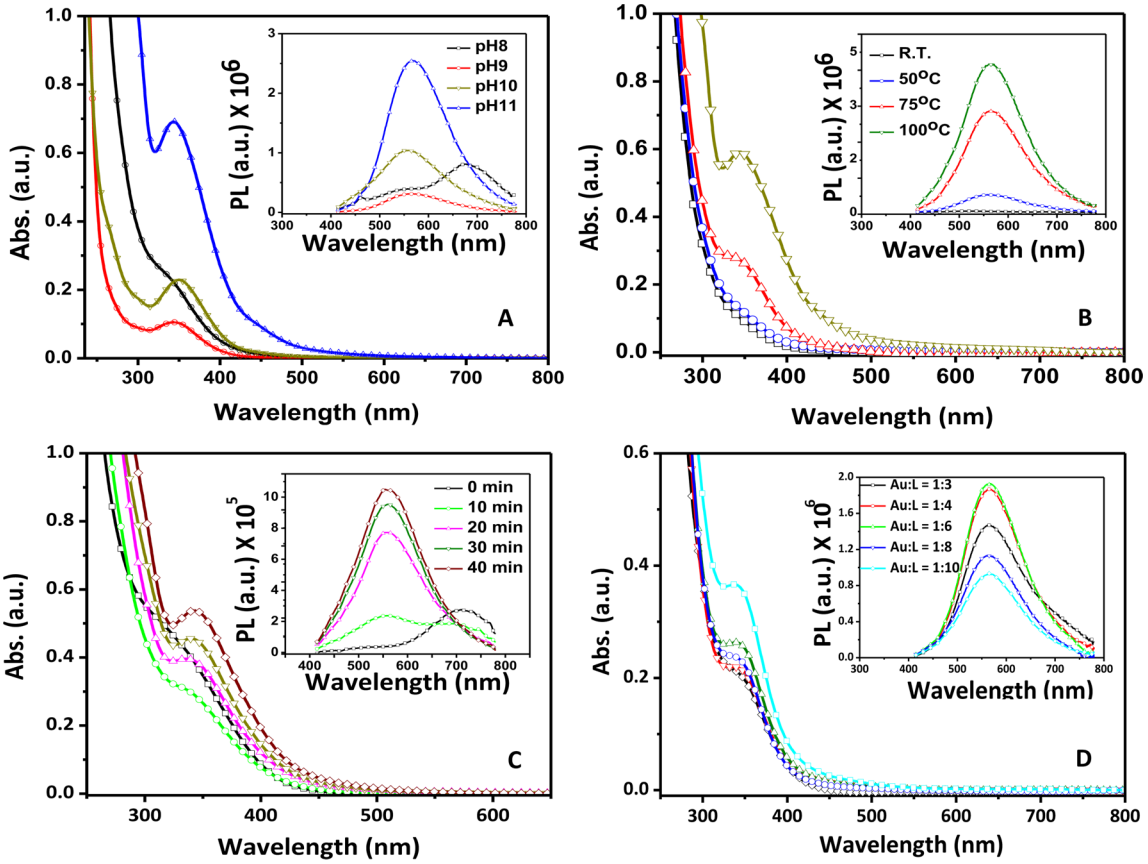

Figure 2. Optimization of the growth conditions. (A) Effect of pH on the fluorescence intensity after 2 h of reaction. (B) Effect of reaction temperature on the fluorescence intensity after 2 h of reaction. (C) Effect of ligand irradiation time on the absorption and PL spectra. (D) Effects of gold-to-ligand precursor molar ratio on the absorption and PL spectra. Growth under refluxing conditions (at 100 °C) was used in (A, C, D) (fluorescence emission spectra collected using 400 nm excitation).

conditions). We limited our focus to this narrow pH window because we know from previous studies, using $NaBH_4$ reduction in the presence of LA-PEG ligands, that growth of NPs and NCs is achieved in alkaline solutions.[41,43,44] Base has been shown to deprotonate thiol groups and thus can increase the coordination interaction of the ligand. Furthermore, we maintained the Au:L* ratio at 1:6 and used UV irradiation of the ligand for 40 min and refluxing conditions (100 °C); L* designates the photochemically excited LA-PEG-OCH_3. Under these conditions, a fluorescence signal was measured for all explored pHs. Nonetheless, consistent high emission centered at ∼560−570 nm was measured when the medium pH was maintained at pH > 9, and the growth was stopped after 2 h. Moreover, we measured a progressive increase in the fluorescence intensity with increasing pH with the highest values measured at pH 11 (see Figure 2A). We also found that under excess ligand conditions and a growth period limited to 2 h using pH 11 the retrieved clusters exhibited a yellow emission with an intensity that strongly depended on the growth temperature used. Figure 2B shows a compilation of spectra collected using growth temperatures ranging from room temperature (RT) to refluxing conditions (100 °C); a substantial increase in the measured intensity (ca. a factor 10) was measured when the growth temperature increased from ∼25 to 100 °C. In the following we maintained the reaction medium at pH 11 and used refluxing conditions at 100 °C, while adjusting all the other relevant parameters.

Effects of UV Irradiation Time. We then probed the effects of changing the ligand irradiation time on the cluster formation and the corresponding photophysical properties. Here we used refluxing conditions for 2 h and ligand solutions that have been UV-irradiated for 0, 5, 10, 20, 30, and 40 min while maintaining Au:L* = 1:6. The cluster dispersions were retrieved after 2 h, and the absorption and fluorescence spectra were collected. Data show that in the absence of UV irradiation a featureless absorption along with broad but weak emission progressively builds up (Figure 2C). This emission is different from that measured for clusters grown using $NaBH_4$ reduction of nonirradiated ligands, where a PL peak at 740 nm was measured.[44] We also found that when the ligand irradiation time was increased, there was a buildup of an absorption peak at 350 nm along with a shift of the emission to yellow combined with a substantial increase in the PL intensity. The shift in the emission to yellow occurred within the first 2−3 h of refluxing for all samples prepared with ligands irradiated for 10 min or longer (Figure 2C). We found that longer irradiation time had little to no effect on the growth or materials quality.

Effects of Au-to-Ligand Ratio. We investigated the effects of changing the molar ratio of Au:L* from 1:3 to 1:10 on the PL, while maintaining the solution at pH 11 and UV irradiation time of the ligands at 40 min. We found that the fluorescence intensities collected from the resulting AuNCs varied greatly, with the highest yields obtained for ratios between 1:4 and 1:6 (see Figure 2D). Higher ratios (e.g., Au:L* = 1:8 and 1:10) yielded materials with lower emission.

DOI: 10.1021/acs.langmuir.6b00950
Langmuir 2016, 32, 6445−6458

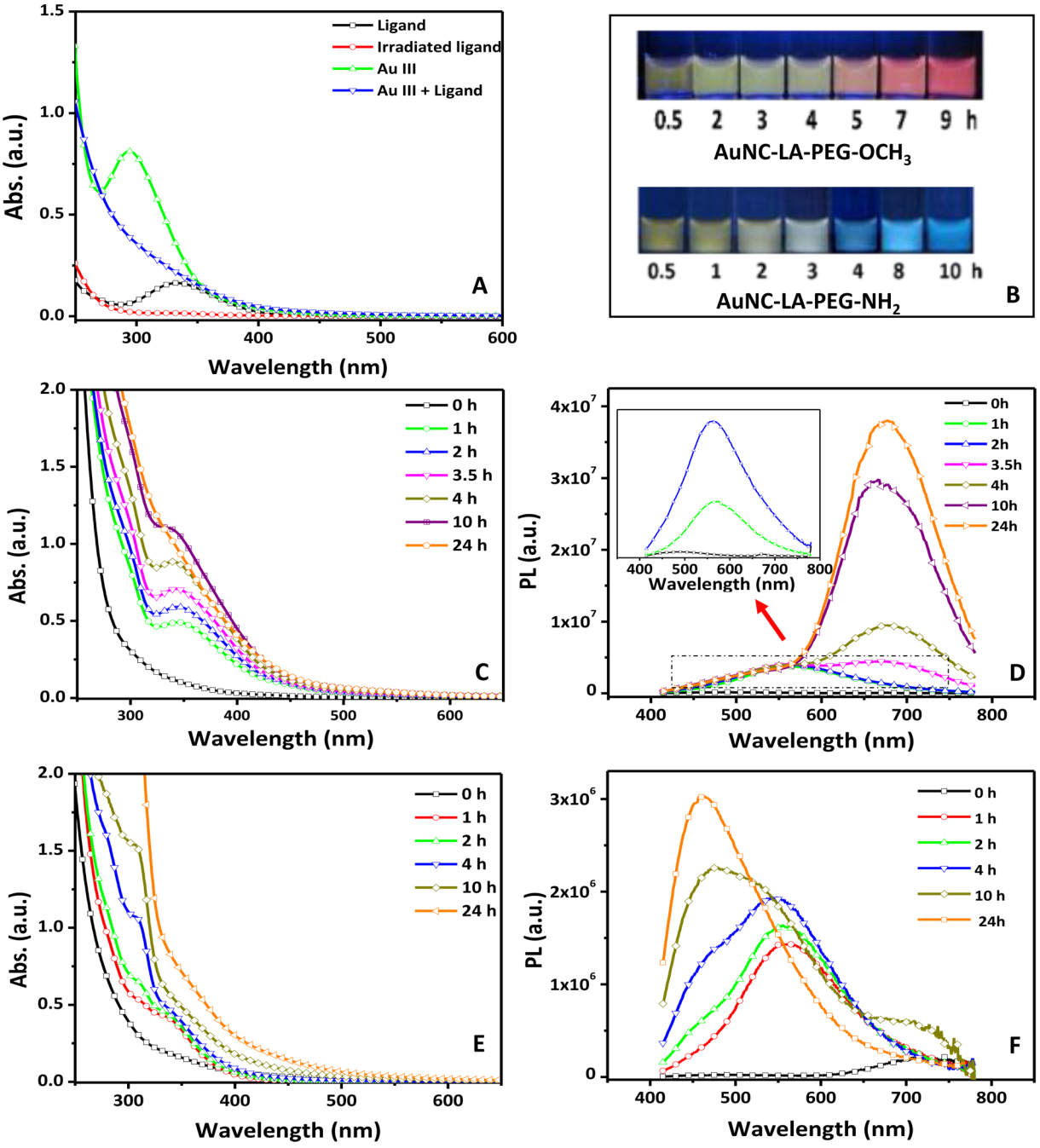

Figure 3. (A) Absorbance spectra collected from the ligand before irradiation (3 mM), ligand after irradiation (for 40 min), and from gold(III) solution (0.5 mM) and gold−ligand reaction mixture before initiation of reaction. (B) Fluorescence of solutions retrieved at different time intervals (as indicated) illuminated using a hand-held UV-lamp (excitation 365 nm). (C, D) Time progression of UV−vis absorption and emission spectra collected from the growth solutions using preirradiated LA-PEG_{750}-OCH_3 (L*) from 0.5 to 24 h. The emission spectra collected from reaction media between 0 and 3 h (depicted separately, D, inset) show that the emission is distinctly yellow during this time. (E, F) UV−vis absorption and emission spectra for the time progression of the growth solution using preirradiated LA-PEG_{600}-NH_2 (L_{amine}*).

Effects of Refluxing Time. Finally, we tracked the growth of the clusters with time under refluxing conditions from the starting point (mixing of the precursors) until 24 h. We started by mixing a solution of LA-PEG_{750}-OCH_3, irradiated for 40 min, with the gold precursor at Au:L* = 1:6. The pH of the medium was adjusted to pH 11 by adding a few drops of aqueous NaOH solution. Before adjusting the temperature and immediately following mixing, the solution turned brownish then pale after several minutes of stirring. Figure 3A shows side-by-side the absorption spectra collected from a gold(III) solution, a solution of the oxidized ligand (LA-PEG-OCH_3, L), a solution of the UV-irradiated ligand (L*), and a mixture of gold(III) and L*. Data show that the usual absorption feature of LA-PEG-OCH_3 at 335 nm and the broad peak at 295 nm for the Au(III) solution have disappeared in the spectrum of the mixture. A concomitant featureless absorption curve that increases from the visible to the UV region was measured for the mixture of L*-plus-Au(III) solution. When the temperature was adjusted to 100 °C and the mixture was left refluxing while stirring, the solution began to change color with time,

DOI: 10.1021/acs.langmuir.6b00950
Langmuir 2016, 32, 6445−6458

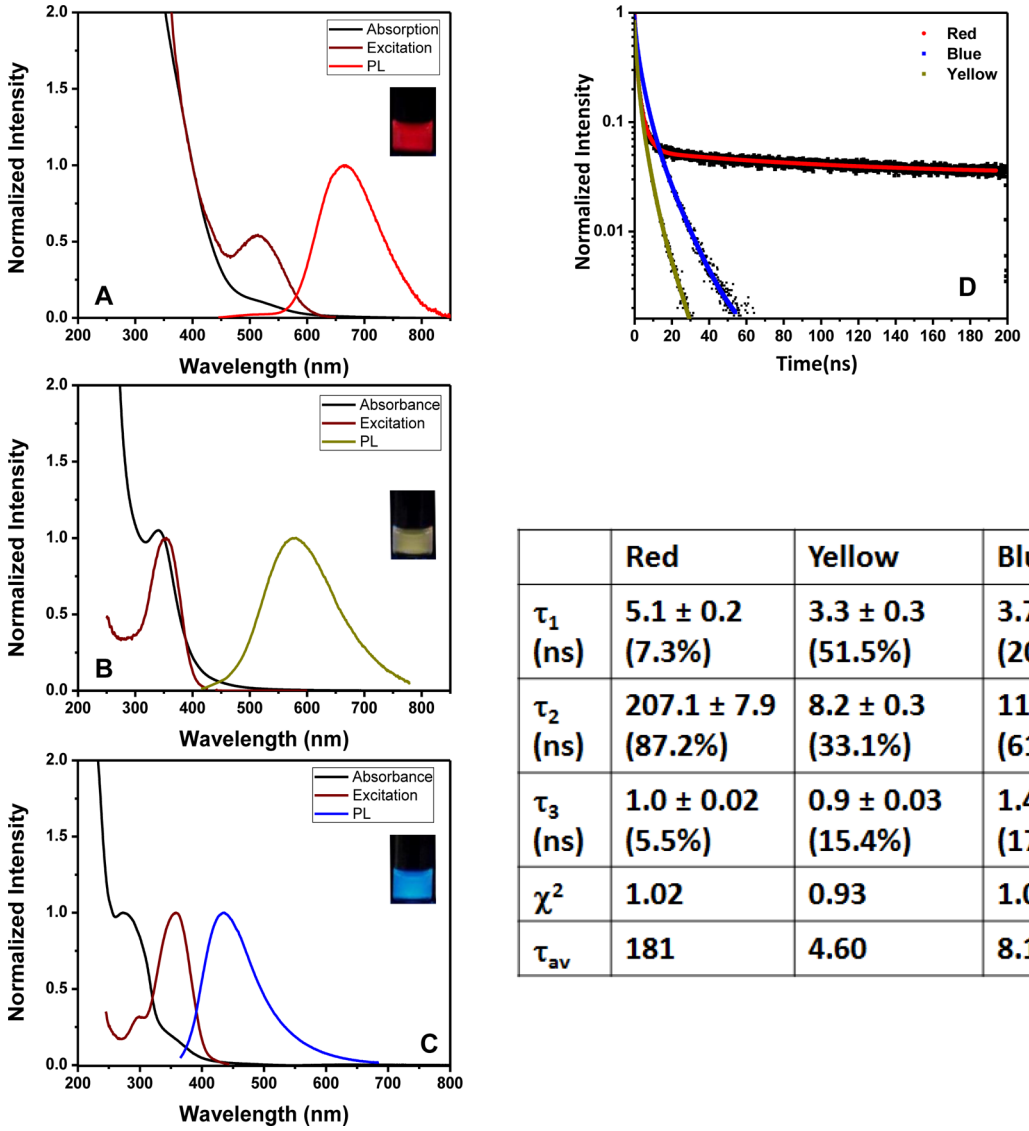

	Red	Yellow	Blue
τ_1 (ns)	5.1 ± 0.2 (7.3%)	3.3 ± 0.3 (51.5%)	3.7 ± 2.6 (20.4%)
τ_2 (ns)	207.1 ± 7.9 (87.2%)	8.2 ± 0.3 (33.1%)	11.5 ± 1.4 (61.8%)
τ_3 (ns)	1.0 ± 0.02 (5.5%)	0.9 ± 0.03 (15.4%)	1.4 ± 0.1 (17.9%)
χ^2	1.02	0.93	1.04
τ_{av}	181	4.60	8.10

Figure 4. Normalized absorption, excitation, and photoluminescence spectra of (A) red-, (B) yellow-, and (C) blue-emitting AuNCs. The PL spectra were collected using excitation at 400 nm for the red- and yellow-emitting clusters and 350 nm for the blue-emitting clusters. The absorption data were normalized with respect to the value at 400 nm for the red clusters and the value at 350 nm for the yellow and blue clusters. The PL was normalized with respect to the peak value for all samples. Fluorescence images showing distinct emission colors of the as-prepared AuNCs excited with hand-held UV lamp (365 nm) are also shown (see insets). (D) Time-resolved fluorescence decay curves for the blue-, yellow-, and red-emitting AuNCs, along with the amplitude weighted lifetimes, fitted with a three-exponential function (eq 1). Calculated average lifetimes are 8.1 ns for blue AuNCs, 4.5 ns for yellow AuNCs, and 181 ns for red AuNCs.

developing a yellow color after 2 h and then turning light brownish and finally brown at the end of the reaction (after ~24 h). Figure 3B shows the fluorescence images from several vials containing aliquots of the corresponding growth solutions illuminated with a hand-held UV-lamp (365 nm excitation); this provides a visual account for the spectral progression with time. The growth was also monitored by periodically retrieving aliquots from the reaction mixture and recording the absorption and emission spectra. Figure 3C,D shows the progression of the spectra collected from materials grown using LA-PEG-OCH_3 under refluxing conditions (100 °C). Initially, a weak absorption feature around 350 nm superposed over a continuously increasing background was measured. In addition, though the intensity of the absorption spectra increased with time, the feature at 350 nm progressively became weaker and morphed into a shoulder after overnight refluxing. The emission also changed with time. The solution started to emit a yellow signal within 30 min, and then the intensity progressively increased with time for up to 2 h of growth. After ~3 h, a red contribution to the measured spectrum started to appear, and the emission progressively shifted from yellow to red (emission peak at ~670 nm). Overall, most of the changes in the absorption and PL spectra occurred within the first 12 h of growth and slowly reach saturation after 24 h. We have monitored the growth solution for up to 24 h to ensure completion of the cluster growth. When the temperature of the reaction mixture was lowered, the growth kinetics became slower, with buildup of the yellow emission requiring growth for a longer time. For example, when growth was carried out at room temperature, the solution still emitted yellow light after a few days and did not fully become red-emitting even after 4 weeks.

DOI: 10.1021/acs.langmuir.6b00950
Langmuir 2016, 32, 6445−6458

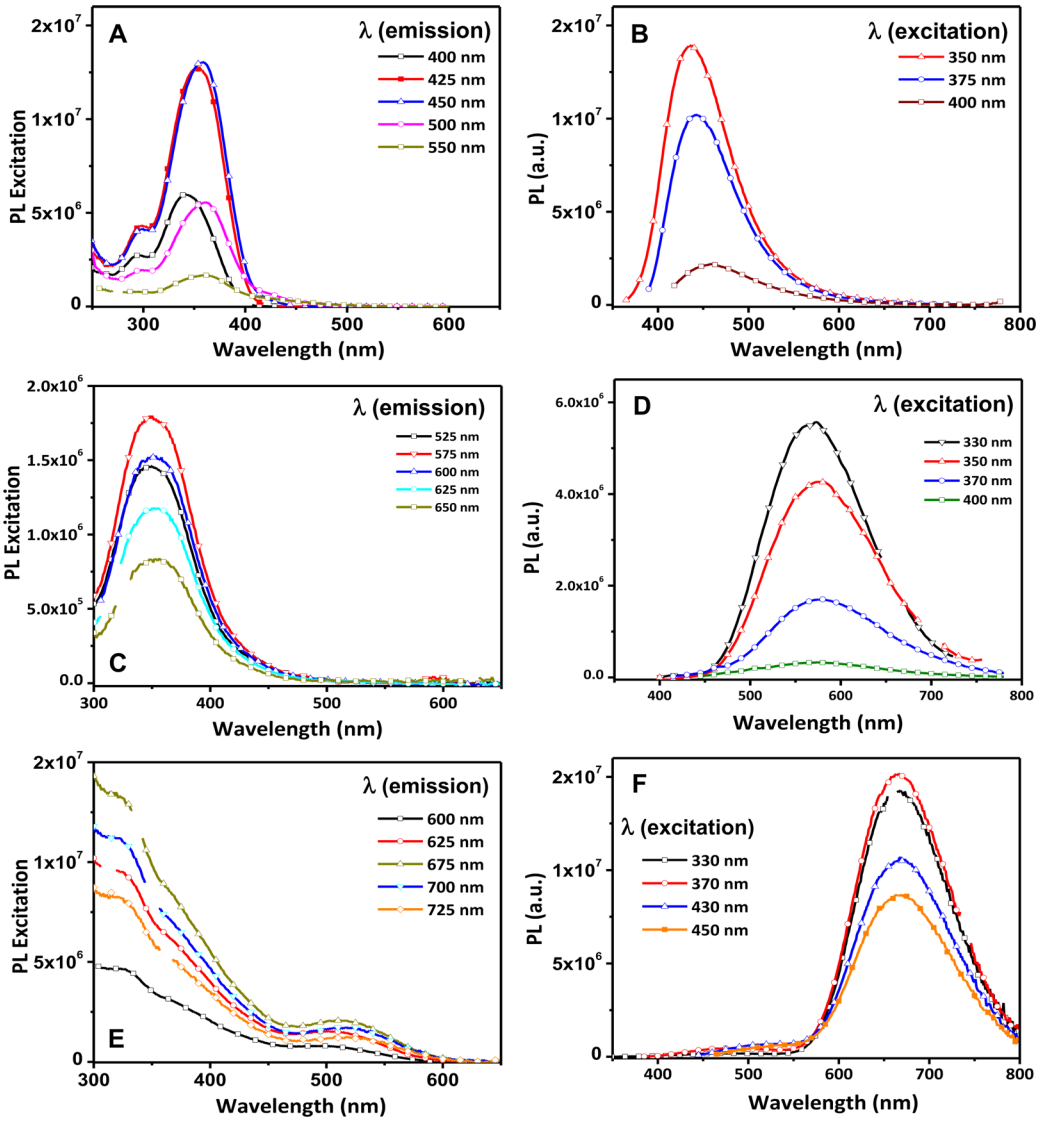

Figure 5. (A, C, E) Excitation spectra of the blue-, yellow-, and red-emitting AuNCs using detection at the indicated emission wavelengths. (B, D, F) PL spectra of the same three sets of AuNCs collected using excitation at the indicated wavelengths. The second overtone contribution signals (e.g., contribution at 800 nm for excitation at 400 nm) in both sets of spectra have been manually removed. Note the excitation spectra were limited to $\lambda \geq 300$ nm for the yellow and red clusters.

Growth of Blue-Emitting Clusters in the Presence of Ligands Terminated with $-NH_2$ Groups. We also carried out the same growth using LA-PEG ligands terminated with two reactive functional groups, namely, $-COOH$ and $-NH_2$ (PEG MW = 600 g/mol). We found that with either ligand yellow-emitting AuNCs were formed within 2 h, as was the case of LA-PEG-OCH_3 (see Figure S3). However, the growth behavior observed for reactions involving these ligands and over an extended period was different from what we detailed above. We found that overnight refluxing of a solution containing Au precursor and UV-irradiated LA-PEG-NH_2 (L_{amine}*) yielded totally different emission and absorption features, as shown in Figure 3E,F. In particular, the spectra shown in Figure 3E indicate that the broad absorption feature around 350 nm, measured after ∼2 h of growth, progressively disappeared, while a second feature appeared around 300 nm. Conversely, the fluorescence spectra show a net blue-shift of the emission peak with time from ∼565 to ∼460 nm (Figure 3F). These data clearly indicate that the presence of a reactive amine group in the ligand alters the nature of the formed clusters, with the buildup of a well-defined blue emission for reaction involving L_{amine}*. To further confirm that the net blue-shift in the emission was triggered by the presence of an amine-reactive group, we carried out the growth reaction using UV-irradiated LA-ethylenediamine (L_{EDA}*). As L_{EDA} (oxidized form) is insoluble in water, irradiation of the ligand was first carried out in methanol solution, and then this irradiated ligand solution was added to a mixture of Au precursor followed by growth under basic conditions. Here too we observed blue-shift of the emission peak after overnight refluxing (see Figure S4). Similarly, when the reaction was carried out using a mixture of L* and EDA, a spectrum exhibiting a bimodal emission with blue-green (peak at 500 nm) and red (peak at 695 nm) contributions was measured after overnight refluxing (see Figure S4). Finally, to test whether the distinct blue-shift observed for the reaction mixture containing L_{amine}* is an inherent property associated with the growth conditions, we mixed a purified red-emitting NC dispersion (prepared with

DOI: 10.1021/acs.langmuir.6b00950
Langmuir 2016, 32, 6445−6458

L*) with large excess of L_{amine}* and let incubate overnight while stirring at 100 °C. We found that they induced a shift in the emission from red to blue (see Figure S5). In comparison, the emission spectra collected from solutions prepared using UV-irradiated LA-PEG-COOH (L_{COOH}*) under overnight refluxing conditions showed bimodal emission, with shoulders at ≈445 and 540 nm, and no clear trend was observed (see Figure S6). These results clearly show that the fate of the grown clusters is ligand-dependent. For instance, LA-PEG-OCH_3 ligand which is terminated with inert group produces AuNCs with emission that drifts overnight to the red. This implies that ligands with an inert terminal group facilitate the continuous growth of the NCs with emission shifting from yellow to red. Conversely, introducing reactive groups during growth (in particular, LA-PEG-NH_2, or ligand mixed with primary amine-containing molecules) have the opposite effect on the growth process; i.e., the emission shifts from yellow to blue. Furthermore, the estimated hydrodynamic sizes of these clusters (discussed below) indicate that blue-emitting clusters are indeed smaller than yellow- and red-emitting NCs, which is consistent with the observed shift in emission collected from those materials.

Spectroscopic Characterization. Figure 4A–C shows the optical absorption, excitation, and emission spectra collected from dispersions of the three sets of NCs after purification. The PL excitation spectrum of the red-emitting AuNCs shows an excitation peak at 510 nm, a feature that is not well-defined in the absorption spectrum of the NCs. In comparison, the excitation spectra of the yellow- and blue-emitting AuNCs show a well-defined peak around 350 nm that coincides with the weak feature measured in the absorption spectra. The photoluminescence spectra show that the emission maxima for the red-, yellow-, and blue-emitting NCs are at ∼670, ∼570, and ∼440 nm, respectively. The quantum yields of the AuNCs were measured using standard references; Rhodamine 6G (QY in ethanol = 95%) was used as a standard for the yellow and red NCs, whereas the quantum yield of blue NCs was measured using DAPI (QY in water = 4%) as a standard. The measured quantum yields of the red-, yellow-, and blue-emitting samples were ∼7.5%, ∼3%, and ∼4.2%, respectively.

The time-resolved fluorescence decay profiles collected from dispersions of the three sets of clusters are shown in Figure 4D. The fluorescence lifetimes were extracted using a three-exponential fit of the fluorescence decay curves, using eqs 1 and 2. The table shown in Figure 4 lists the individual components extracted from the fit for each set. An average lifetime (extracted using eq 2) of 181, 4.6, and 8.1 ns was measured for the red-, yellow-, and blue-emitting dispersions, respectively. The average fluorescence lifetime of the red-emitting clusters is substantially longer than those measured for the blue and yellow clusters. However, a close look at the three lifetime components extracted from the fit indicates that τ_1 and τ_3 are similar for all the three sets. However, τ_2 is much longer for the red-emitting clusters, indicating that this lifetime is the major source of the difference measured in the average lifetimes. We should note that the time-resolved florescence features measured for the present red-emitting clusters are very similar to those observed for the clusters prepared using $NaBH_4$ reduction (those clusters emit slightly farther in the red), detailed in ref 44. Rather long lifetimes have also been reported for other red-emitting clusters prepared using other thiolate ligands.[32,53] Such long fluorescence lifetimes, commonly reported for red and NIR-emitting clusters, has been attributed to a dominant role of ligand-to-metal charge transfer states.

We further investigated the nature of the fluorescence emission by collecting several excitation scans using distinct detection lines across the PL spectrum as well as several PL emission spectra generated by exciting the sample at different wavelengths across the absorption profile. The data for the red, yellow and blue clusters are summarized in Figure 5. All PL spectra were generated using similar excitation lines within the 300–500 nm range. Data indicate that for the yellow- and red-emitting clusters there is no change in the excitation maximum irrespective of the wavelength at which emission was collected, implying that the emission arises from a single population of emitting species. Conversely, when the excitation was varied, the shape of the emission spectra collected from both sets of clusters was not affected. The overall PL intensity tracked the absorbance value at the excitation wavelength used, with higher PL measured for the larger absorption, and vice versa (Figure 5). This implies that for both sets, the emitting species in the sample are all efficiently excited at the excitation range 300–500 nm. In comparison, the spectra collected for the blue clusters exhibit a slight dependence of the PL on the excitation line, while the shape of excitation scan also slightly varied depending on the PL detection line. The features observed for the blue clusters need to be coupled with the fact that excitation of the samples coincided with the tail of the absorption spectrum, i.e., excitation at the red edge of the absorption spectrum (see Figures 3E and 4C). This selectively excites a subpopulation of clusters in the dispersion with emission over the red edge of the spectrum; this results in a slight red-shift in the collected florescence spectrum. This feature is similar to the fluorescence line narrowing (FLN) widely explored for luminescent QDs.[54] The fluorescence line narrowing features are rather mild here with absence of any phonon progression, as the sample was excited using UV lamp and the fact the overall PL emission is rather broad compared to those reported for QDs. This aspect merits further exploration and should be probed for all three sets of clusters by for example, exciting the red clusters near 600 nm using a laser line.[54] This can ultimately allow us to probe possible effects of core size and dispersion in cluster size on the PL properties.

The above properties indicate that the three sets of clusters are indeed different in size and potentially composition. When a high energy photon is absorbed, it excites an electron into higher energy states, creating an electron–hole pair (an exciton). The electron rapidly relaxes nonradiatively to the lowest excitation energy before recombining with the hole in the HOMO, resulting in photon emission. This emission often referred to as band-edge emission in semiconducting materials, is consistent with the Kasha principle, which states that fluorescence always emanates from the lowest energy state of a system.[55]

Structural Characterization. The composition of the clusters and the gold–sulfur interactions were probed by X-ray photoelectron spectroscopy (XPS). We monitored the Au 4f binding energies (BE) of the three clusters and compared them to those measured for the Au–DHLA complex and the larger size plasmonic AuNPs (∼5 nm). Figure 6 shows the Au(4f) core-level photoemission spectra collected from thin films made of the Au clusters (red, yellow, and blue) along with the spectra collected from films of Au–DHLA complex and AuNPs, all measured at room temperature. It is clear from the spectra that the 4f BE of the clusters are located between the energies corresponding to AuNPs and Au–DHLA complex. While the BE values of Au(4f) peaks of the AuNPs are closer to Au(0)

DOI: 10.1021/acs.langmuir.6b00950
Langmuir 2016, 32, 6445–6458

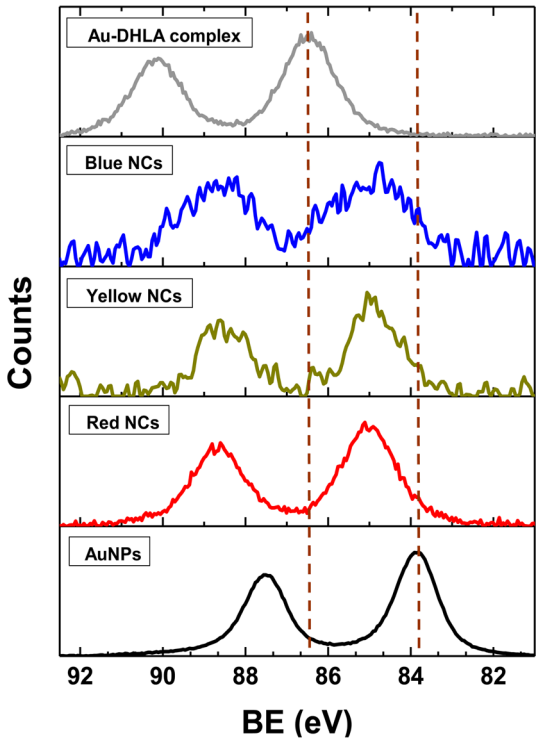

Figure 6. Au 4f XPS spectra of Au−DHLA complex (prepared by mixing DHLA and $HAuCl_4$ solution), blue, yellow, and red clusters and large AuNPs (5 nm, protected by LA-PEG-OCH_3, prepared by borohydride reduction following the procedure in ref 41). The vertical lines from right to left correspond to the Au $4f_{7/2}$ BEs of AuNPs and Au−DHLA complex, respectively.

films and with similar peak widths, those measured for the clusters are considerably broader. The broadening of the Au(4f) peaks has also been attributed to inhomogeneity in the degree of electron donation depending on the binding sites of the ligands.[24,56] We found that the experimental Au($4f_{7/2}$) peaks can be deconvoluted into two components: one originating from the inner and the other from the surface atoms of the gold NCs. Moreover, the Au($4f_{7/2}$) peak position for the inner Au atoms was found to monotonically shift from ∼84.0 to ∼84.5 eV as the cluster size decreased. This is due to the decrease in the kinetic energy of the outgoing photoelectron through the Coulombic attraction between the photocreated hole and the electron (known as "final-state effect").[57] Likewise, the Au($4f_{7/2}$) peak positions of the surface Au atoms are located at higher in energy (∼85 eV), a feature attributed to the electron donation from the surface Au atoms to the thiolates (known as "initial-state effect").[56] Since the Au($4f_{7/2}$) binding energies of the clusters are around 85 eV and most of the Au atoms are located on the core surface for such small clusters, it is reasonable to conclude that the chemical shifts observed here are mostly due to the electron donation from the Au core to the ligands in the clusters, with a smaller contribution from the Au(I)−thiolate complexes near or at the surface. The detailed peak shape analysis of Au 4f spectra are provided in the Supporting Information (Figure S7). Similarly, the BEs of S 2p peaks showed the presence of bound and unbound thiols (data not shown). The typical BE of thiols and disulfides lies between 163 and 164 eV, and after binding on the gold surface, it decreases to 162 eV. Sulfur peaks were also present at higher BE (166−169 eV), possibly due to some oxidized sulfur species.

We have attempted to characterize the AuNCs using mass spectroscopy measurements, namely matrix-assisted laser desorption/ionization (MALDI) and TEM. We were not able to extract any reliable mass data, as the collected MALDI spectra were dominated by the signature and polydispersity of the PEG ligands. Conversely, TEM imaging was only able to resolve the size of the red-emitting AuNCs (TEM size 1.4 ± 0.2 nm, Figure 7A), but no data could be collected from the blue-

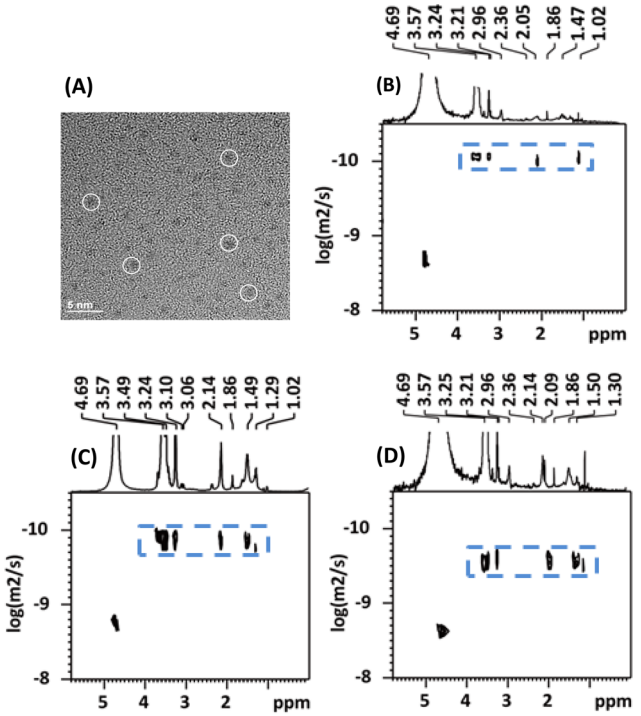

Figure 7. (a) TEM image of red-emitting AuNCs (size 1.4 ± 0.2 nm, horizontal bar corresponding to 5 nm.), (b, c, d) DOSY spectra of red-, yellow-, and blue-emitting AuNCs, respectively (D_2O, 600 MHz, 294 K). The diffusion coefficient of water molecules in the three samples are the same, with the value of 1.8×10^{-9} m^2/s.

and yellow-emitting AuNCs. The size extracted for the red-emitting clusters was very close to that measured for the materials grown using borohydride reduction in the presence of LA-PEG-OCH_3 and LA-zwitterion ligands.[44]

We have, however, successfully applied diffusion ordered NMR spectroscopy (DOSY NMR) to measure the hydrodynamic size of the three sets of AuNCs. DOSY is a versatile technique and offers an alternative to dynamic light scattering, which is not able to resolve subnanometer objects in a solution. Indeed, DOSY has recently emerged as a powerful, non-destructive technique to extract accurate information about the diffusion coefficient, *D*, of molecules and nanoparticles in solutions. This technique exploits the time-dependent signature of an NMR active atom (e.g., ^1H, ^{13}C, or ^{31}P) in a molecule of interest dispersed in a deuterated solution (aqueous or organic). A few groups have successfully used DOSY ^1H NMR spectroscopy to characterize the ligand environment and symmetry of thiolate-protected gold nanoclusters.[58] The diffusion coefficient of molecules of interest in the solution is correlated with their hydrodynamic size, R_H. It also depends on the nature of the soluble object, effective size, and shape via the

DOI: 10.1021/acs.langmuir.6b00950
Langmuir 2016, 32, 6445−6458

Stokes−Einstein equation. In particular, for a homogeneous dispersion of spherical molecules that equation is expressed as

$$R_H = \frac{k_B T}{6\pi\eta D} \quad (4)$$

where k_B is the Boltzmann constant, T is the temperature, η is the viscosity of the medium, and D is the diffusion coefficient of the objects. DOSY NMR has recently been used by Häkkinnen and co-workers to determine the hydrodynamic size of three well-characterized phenylethanethiol (PET)-stabilized gold nanoclusters $Au_{25}(PET)_{18}$, $Au_{38}(PET)_{24}$, and $Au_{144}(PET)_{60}$.[58]

We applied this technique to estimate the diffusion coefficients and hydrodynamic radii for our red-, yellow-, and blue-emitting AuNCs. Figure 7 shows the 2D DOSY ^{1}H NMR spectra collected from dispersions of the clusters dispersed in D_2O and plotted as log(D) vs ^{1}H NMR chemical shifts, associated with specific protons of the ligands (e.g., methylene protons at 3.57 ppm and the solvent is located at 4.69 ppm). The data show that the diffusion coefficient measured is the same regardless of which proton signature (in the bound ligand) is probed, indicating that we are indeed probing protons from bound ligand molecules. Furthermore, there is a clear difference in the diffusion coefficients measured for the three sets of clusters (Table 1). The values of R_H confirm that

Table 1. Values of the Diffusion Coefficients, D, Extracted from the DOSY NMR Measurements (Average ± SD) along with the Corresponding Hydrodynamic Radii, R_H (nm), Calculated from the Stokes−Einstein Equation, for the Three Set of AuNCs[a]

cluster	D (m^2/s)	R_H (nm)
red	$(7.20 \pm 0.14) \times 10^{-11}$	3.00
yellow	$(1.25 \pm 0.10) \times 10^{-10}$	1.59
blue	$(2.95 \pm 0.24) \times 10^{-10}$	0.76

[a]Average D was used for the calculation of R_H. The data were collected at 294 K in D_2O. Viscosity of water = 0.99 mPa·s (or cP). The obtained D for the water molecules in the three sets of AuNCs are 1.8×10^{-9} m^2/s.

the sizes measured for the clusters closely track the anticipated trend based on the absorption and PL data, with R_H(red) > R_H(yellow) > R_H(blue). The hydrodynamic sizes extracted for the yellow and, in particular, the blue-emitting clusters should be viewed only as approximate estimates. Indeed, the purification steps applied to those two samples were slightly different. Because of their small size, removal of the free ligands did not rely on the use of 10 kDa membrane filtration devices as was done for the red-emitting materials. Instead, we employed PD10 columns which may not be as effective in removing all the free ligands from the growth solutions. As such, the samples used for characterization may ultimately have rather large concentrations of free ligands. These free ligands likely dominate the DOSY NMR signal, yielding rather small hydrodynamic size. The error may be more acute for the blue emitting materials. In fact, DOSY NMR applied to LA-PEG_{750}-OCH_3 ligands yielded $R_H \sim 1$ nm, which is slightly larger than the one measured for the blue sample ($R_H \sim 0.76$) or that expected for LA-PEG_{600}-NH_2 ($R_H \sim 0.6$−0.7 nm) used for preparing the blue samples.

We would like to note that for the red cluster we find that $R_H/R_{TEM} \sim 3$. The larger hydrodynamic size compared to that from TEM is expected, as the former accounts for contributions from hydrodynamic interactions combined with the presence of the LA-PEG ligand on the cluster surfaces. Both contributions tend to yield larger hydrodynamic radius compared to dimensions extracted form TEM or X-ray scattering, for example. This is also consistent with data on larger size nanoparticles.

Colloidal Stability. We should note that these NCs can also be dried (under vacuum) and redispersed in organic solvents, which expands the processing conditions of these materials. Indeed, due to the amphiphilic nature of the PEG coating, the prepared clusters can be readily dispersed in both buffer as well as organic solutions.[44] While the absorption and emission properties of the blue- and red-emitting clusters are preserved following transfer to organic solvents (e.g., chloroform), we found that the yellow-emitting clusters exhibited a clear solvatochromic effect. More precisely, the cluster emission peak was blue-shifted from ∼565 nm in water to ∼500 nm in chloroform (changing the solution color from yellowish to greenish; see Figure 8). It is understood that in molecular

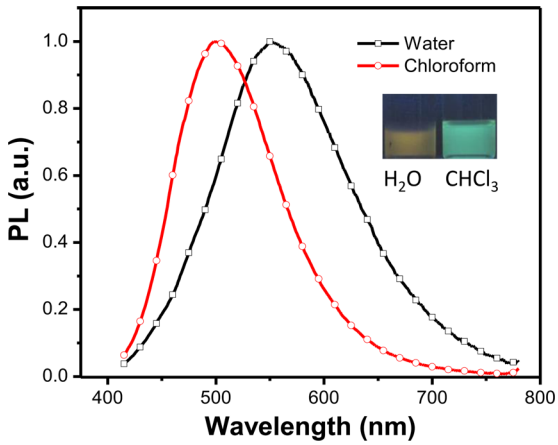

Figure 8. Solvatochromic effect of yellow-emitting AuNCs in water and in chloroform. The emission maximum is at 560 and 500 nm, respectively; samples were excited at 400 nm. Images of the solutions in water and chloroform under UV-exposure are shown together.

systems solvatochromic effects arise from contributions of dipole−dipole, dipole−induced dipole, or dispersion interactions with solvent molecules, which results in differential solvation and stabilization of ground and excited states.[59] If the ground state is more stable than the excited state upon solvation, negative solvatochromism (blue-shift) will occur, whereas if the excited state is more stable than the ground state, positive solvatochromism (red-shift) will occur upon excitation. Solvatochromism has also been observed in colloidal quantum dots and was correlated to the dielectric environment that perturbs the energy of the quantum confined exciton.[60] Solvatochromic effect of yellow-emitting samples may be related to the transient nature of these clusters. We showed above that these clusters, usually collected after 2−3 h of growth, somewhat constitute intermediate state between the red- and blue-emitting materials reached after overnight refluxing. We also tested the pH stability of the clusters in PBS buffer (50 mM, pH 2−12). The strong interaction between Au and S atoms along with a long hydrophilic PEG segment provides greater colloidal stability to these clusters. Our study indicates that these nanoclusters are stable in a wide range of pH up to 1 year, with no signs of aggregation, although

DOI: 10.1021/acs.langmuir.6b00950
Langmuir 2016, 32, 6445−6458

the yellow-emitting clusters lost their fluorescence within 4−6 weeks of storage at 4 °C. The fluorescence of blue- and red-emitting clusters was maintained over the entire period of storage. Additional data on the colloidal stability tests are provided in the Supporting Information (see Figure S8).

The use of photochemically modified LA-PEG ligands, combined with reaction kinetics that do not rely on a chemical reducing agent, has indeed altered the growth reaction and produced fluorescent clusters that could not be accessed before. This contrasts with the growth under borohydride reducing conditions (using $HAuCl_4{\cdot}3H_2O$ and molar excess ligands), which produced only red-emitting clusters.[44] This may be attributed to a different reactivity of the UV-irradiated ligands toward Au(III) (compared with the oxidized form) and a slowing of the growth kinetics. The formation of the smaller size yellow-emitting clusters during the first 2 h of growth, followed by the shift of the emission to red (e.g., in the presence of L*) coupled with increase in cluster size at longer time, is expected for colloidal nanomaterials. However, the appearance of blue-shift in the emission accompanied by reduction in cluster size, as measured by DOSY-NMR, when photoirradiated and amine-terminated ligands are used seems to be "counterintuitive". It indicates that the amine groups may be strongly interacting with radical sulfur groups formed during UV-irradiation of the dithiolane ring.[48] At this point we do not have a solid chemical rationale to what exactly happens to the reaction and how the presence of amine groups promotes reduction in cluster size with growth time, instead of the "expected" increase in size and red-shift in the PL emission. We are exploring ideas and possible rationales to understand what exactly happens to the growth when amine-modified ligands are used. We hope to develop a convincing rationale and report on its fundamentals in future works.

CONCLUSION

We have developed a new strategy to prepare a set of size- and emission-tunable nanocrystals composed of gold cores (Au nanoclusters), stabilized with multifunctional ligands made of lipoic acid anchoring groups appended with poly(ethylene glycol) hydrophilic modules (LA-PEG). We have shown that the photochemically transformed LA-PEG ligands combined with refluxing conditions and alkaline medium (pH = 11) are required for the growth of high quality AuNCs with tunable fluorescence. Both photoirradiated LA-PEG terminated by methoxy or amine segments ($-OCH_3$ or NH_2) have yielded yellow-emitting clusters with an emission centered around 560−570 nm during the first stage of the reaction (2 h). However, prolonged reaction time at 100 °C yielded blue-emitting and red-emitting AuNCs when using LA-PEG-NH_2 and LA-PEG-OCH_3, respectively. XPS measurements showed that the Au($4f_{7/2}$) binding energy of the clusters lays between those of metallic films and Au complexes, indicating the presence of both core Au(0) together with surface Au(I) atoms in the cluster structure. Overall, the binding energies were found to be similar to the reported values for other ultrasmall clusters. XPS measurements also confirmed the presence of gold-to-thiol interactions. Additionally, hydrodynamic size measurements using the DOSY-NMR technique indicated that the size measured for these clusters decreased from red to yellow to blue. TEM characterization also indicates that these clusters are very small with a radius of ∼1 nm or smaller. This aqueous phase growth of AuNCs will be of great interest for researchers seeking tunable-emission nanoclusters stabilized with single scaffold ligands (here LA-PEG ligands), in particular for bioimaging applications where multiple color emission is desirable.

ASSOCIATED CONTENT

Supporting Information

The Supporting Information is available free of charge on the ACS Publications website at DOI: 10.1021/acs.langmuir.6b00950.

Additional data and experimental details on the effect of ligand irradiation, optimization of synthesis, effect of functional groups, synthesis using various amine ligands, ligand exchange of red-emitting AuNCs with LA-PEG-NH_2, multiple PL excitation scans along with excitation-dependent emission spectra, XPS spectra, and colloidal stability tests (PDF)

AUTHOR INFORMATION

Corresponding Author

*E-mail: mattoussi@chem.fsu.edu (H.M.).

Notes

The authors declare no competing financial interest.

ACKNOWLEDGMENTS

The authors thank the National Science Foundation for financial support (NSF-CHE #1508501 and #1058957). They also acknowledge the Joint Funding for Promoting the Scientific Collaboration Across the Strait (China, Grant U1205113). We thank the National High Magnetic Field Laboratory for TEM work, the FSU Physics facility for the assistance with XPS measurements, and Dr. Banghao Chen (FSU Chemistry, NMR facility) for the assistance with DOSY experiments.

REFERENCES

(1) Wu, Z.; Jin, R. On the Ligand's Role in the Fluorescence of Gold Nanoclusters. *Nano Lett.* **2010**, *10* (7), 2568−2573.

(2) Li, L. L.; Liu, H. Y.; Shen, Y. Y.; Zhang, J. R.; Zhu, J. J. Electrogenerated Chemiluminescence of Au Nanoclusters for the Detection of Dopamine. *Anal. Chem.* **2011**, *83* (3), 661−665.

(3) Lin, C. A. J.; Lee, C. H.; Hsieh, J. T.; Wang, H. H.; Li, J. K.; Shen, J. L.; Chan, W. H.; Yeh, H. I.; Chang, W. H. Synthesis of Fluorescent Metallic Nanoclusters toward Biomedical Application: Recent Progress and Present Challenges. *J. Med. Biol. Eng.* **2009**, *29* (6), 276−283.

(4) Shiang, Y. C.; Huang, C. C.; Chen, W. Y.; Chen, P. C.; Chang, H. T. Fluorescent gold and silver nanoclusters for the analysis of biopolymers and cell imaging. *J. Mater. Chem.* **2012**, *22* (26), 12972−12982.

(5) de Heer, W. A. The physics of simple metal clusters: experimental aspects and simple models. *Rev. Mod. Phys.* **1993**, *65* (3), 611−676.

(6) Zheng, J.; Nicovich, P. R.; Dickson, R. M. Highly fluorescent noble-metal quantum dots. *Annu. Rev. Phys. Chem.* **2007**, *58*, 409−431.

(7) Muhammed, M. A. H.; Verma, P. K.; Pal, S. K.; Retnakumari, A.; Koyakutty, M.; Nair, S.; Pradeep, T. Luminescent Quantum Clusters of Gold in Bulk by Albumin-Induced Core Etching of Nanoparticles: Metal Ion Sensing, Metal-Enhanced Luminescence, and Biolabeling. *Chem. - Eur. J.* **2010**, *16* (33), 10103−10112.

(8) Park, J.; An, K. J.; Hwang, Y. S.; Park, J. G.; Noh, H. J.; Kim, J. Y.; Park, J. H.; Hwang, N. M.; Hyeon, T. Ultra-large-scale syntheses of monodisperse nanocrystals. *Nat. Mater.* **2004**, *3* (12), 891−895.

(9) Talapin, D. V.; Lee, J. S.; Kovalenko, M. V.; Shevchenko, E. V. Prospects of Colloidal Nanocrystals for Electronic and Optoelectronic Applications. *Chem. Rev.* **2010**, *110* (1), 389−458.

DOI: 10.1021/acs.langmuir.6b00950
Langmuir 2016, 32, 6445−6458

(10) Reiss, P.; Protiere, M.; Li, L. Core/Shell Semiconductor Nanocrystals. *Small* **2009**, *5* (2), 154−168.
(11) Goia, D. V.; Matijevic, E. Tailoring the particle size of monodispersed colloidal gold. *Colloids Surf., A* **1999**, *146* (1−3), 139−152.
(12) Goia, D. V. Preparation and formation mechanisms of uniform metallic particles in homogeneous solutions. *J. Mater. Chem.* **2004**, *14* (4), 451−458.
(13) Duan, H. W.; Nie, S. M. Etching colloidal gold nanocrystals with hyperbranched and multivalent polymers: A new route to fluorescent and water-soluble atomic clusters. *J. Am. Chem. Soc.* **2007**, *129* (9), 2412−2413.
(14) Lin, C. A. J.; Yang, T. Y.; Lee, C. H.; Huang, S. H.; Sperling, R. A.; Zanella, M.; Li, J. K.; Shen, J. L.; Wang, H. H.; Yeh, H. I.; Parak, W. J.; Chang, W. H. Synthesis, Characterization, and Bioconjugation of Fluorescent Gold Nanoclusters toward Biological Labeling Applications. *ACS Nano* **2009**, *3* (2), 395−401.
(15) Shang, L.; Azadfar, N.; Stockmar, F.; Send, W.; Trouillet, V.; Bruns, M.; Gerthsen, D.; Nienhaus, G. U. One-Pot Synthesis of Near-Infrared Fluorescent Gold Clusters for Cellular Fluorescence Lifetime Imaging. *Small* **2011**, *7* (18), 2614−2620.
(16) Yan, L.; Cai, Y. Q.; Zheng, B. Z.; Yuan, H. Y.; Guo, Y.; Xiao, D.; Choi, M. M. F. Microwave-assisted synthesis of BSA-stabilized and HSA-protected gold nanoclusters with red emission. *J. Mater. Chem.* **2012**, *22* (3), 1000−1005.
(17) Liu, H. Y.; Zhang, X. A.; Wu, X. M.; Jiang, L. P.; Burda, C.; Zhu, J. J. Rapid sonochemical synthesis of highly luminescent non-toxic AuNCs and Au@AgNCs and Cu (II) sensing. *Chem. Commun.* **2011**, *47* (14), 4237−4239.
(18) Huang, C. C.; Liao, H. Y.; Shiang, Y. C.; Lin, Z. H.; Yang, Z.; Chang, H. T. Synthesis of wavelength-tunable luminescent gold and gold/silver nanodots. *J. Mater. Chem.* **2009**, *19* (6), 755−759.
(19) Wang, Z. J.; Cai, W.; Sui, J. H. Blue Luminescence Emitted from Monodisperse Thiolate-Capped Au-11 Clusters. *ChemPhysChem* **2009**, *10* (12), 2012−2015.
(20) Huang, X.; Li, B. Y.; Li, L.; Zhang, H.; Majeed, I.; Hussain, I.; Tan, B. E. Facile Preparation of Highly Blue Fluorescent Metal Nanoclusters in Organic Media. *J. Phys. Chem. C* **2012**, *116* (1), 448−455.
(21) Huang, X.; Luo, Y.; Li, Z.; Li, B. Y.; Zhang, H.; Li, L.; Majeed, I.; Zou, P.; Tan, B. E. Biolabeling Hematopoietic System Cells Using Near-Infrared Fluorescent Gold Nanoclusters. *J. Phys. Chem. C* **2011**, *115* (34), 16753−16763.
(22) Bao, Y. P.; Zhong, C.; Vu, D. M.; Temirov, J. P.; Dyer, R. B.; Martinez, J. S. Nanoparticle-free synthesis of fluorescent gold nanoclusters at physiological temperature. *J. Phys. Chem. C* **2007**, *111* (33), 12194−12198.
(23) Zheng, J.; Dickson, R. M. Individual water-soluble dendrimer-encapsulated silver nanodot fluorescence. *J. Am. Chem. Soc.* **2002**, *124* (47), 13982−13983.
(24) Negishi, Y.; Nobusada, K.; Tsukuda, T. Glutathione-protected gold clusters revisited: Bridging the gap between gold(I)-thiolate complexes and thiolate-protected gold nanocrystals. *J. Am. Chem. Soc.* **2005**, *127* (14), 5261−5270.
(25) Roy, S.; Baral, A.; Bhattacharjee, R.; Jana, B.; Datta, A.; Ghosh, S.; Banerjee, A. Preparation of multi-coloured different sized fluorescent gold clusters from blue to NIR, structural analysis of the blue emitting Au7 cluster, and cell-imaging by the NIR gold cluster. *Nanoscale* **2015**, *7* (5), 1912−1920.
(26) Wang, Y. L.; Chen, J. J.; Irudayaraj, J. Nuclear Targeting Dynamics of Gold Nanoclusters for Enhanced Therapy of HER2(+) Breast Cancer. *ACS Nano* **2011**, *5* (12), 9718−9725.
(27) Xavier, P. L.; Chaudhari, K.; Verma, P. K.; Pal, S. K.; Pradeep, T. Luminescent quantum clusters of gold in transferrin family protein, lactoferrin exhibiting FRET. *Nanoscale* **2010**, *2* (12), 2769−2776.
(28) Chen, Y.; Zheng, X.; Wang, X.; Wang, C.; Ding, Y.; Jiang, X. Near-Infrared Emitting Gold Cluster−Poly(acrylic acid) Hybrid Nanogels. *ACS Macro Lett.* **2014**, *3* (1), 74−76.
(29) Jin, R. C. Quantum sized, thiolate-protected gold nanoclusters. *Nanoscale* **2010**, *2* (3), 343−362.
(30) Wang, S.; Meng, X.; Das, A.; Li, T.; Song, Y.; Cao, T.; Zhu, X.; Zhu, M.; Jin, R. A 200-fold Quantum Yield Boost in the Photoluminescence of Silver-Doped AgxAu25−x Nanoclusters: The 13th Silver Atom Matters. *Angew. Chem., Int. Ed.* **2014**, *53* (9), 2376−2380.
(31) Qian, H.; Zhu, Y.; Jin, R. Atomically precise gold nanocrystal molecules with surface plasmon resonance. *Proc. Natl. Acad. Sci. U. S. A.* **2012**, *109* (3), 696−700.
(32) Yu, Y.; Luo, Z. T.; Chevrier, D. M.; Leong, D. T.; Zhang, P.; Jiang, D. E.; Xie, J. P. Identification of a Highly Luminescent Au-22(SG)(18) Nanocluster. *J. Am. Chem. Soc.* **2014**, *136* (4), 1246−1249.
(33) Xie, J.; Zheng, Y.; Ying, J. Y. Protein-Directed Synthesis of Highly Fluorescent Gold Nanoclusters. *J. Am. Chem. Soc.* **2009**, *131* (3), 888−889.
(34) Dou, X.; Yuan, X.; Yao, Q.; Luo, Z.; Zheng, K.; Xie, J. Facile synthesis of water-soluble Au25-xAgx nanoclusters protected by mono- and bi-thiolate ligands. *Chem. Commun.* **2014**, *50* (56), 7459−7462.
(35) Yuan, X.; Zhang, B.; Luo, Z.; Yao, Q.; Leong, D. T.; Yan, N.; Xie, J. Balancing the Rate of Cluster Growth and Etching for Gram-Scale Synthesis of Thiolate-Protected Au25 Nanoclusters with Atomic Precision. *Angew. Chem., Int. Ed.* **2014**, *53* (18), 4623−4627.
(36) Kennedy, T. A. C.; MacLean, J. L.; Liu, J. W. Blue emitting gold nanoclusters templated by poly-cytosine DNA at low pH and poly-adenine DNA at neutral pH. *Chem. Commun.* **2012**, *48* (54), 6845−6847.
(37) Shang, L.; Dong, S. J.; Nienhaus, G. U. Ultra-small fluorescent metal nanoclusters: Synthesis and biological applications. *Nano Today* **2011**, *6* (4), 401−418.
(38) Liu, J.; Yu, M.; Zhou, C.; Yang, S.; Ning, X.; Zheng, J. Passive Tumor Targeting of Renal-Clearable Luminescent Gold Nanoparticles: Long Tumor Retention and Fast Normal Tissue Clearance. *J. Am. Chem. Soc.* **2013**, *135* (13), 4978−4981.
(39) Liu, J.; Yu, M.; Ning, X.; Zhou, C.; Yang, S.; Zheng, J. PEGylation and Zwitterionization: Pros and Cons in the Renal Clearance and Tumor Targeting of Near-IR-Emitting Gold Nanoparticles. *Angew. Chem., Int. Ed.* **2013**, *52* (48), 12572−12576.
(40) Susumu, K.; Uyeda, H. T.; Medintz, I. L.; Pons, T.; Delehanty, J. B.; Mattoussi, H. Enhancing the stability and biological functionalities of quantum dots via compact multifunctional ligands. *J. Am. Chem. Soc.* **2007**, *129* (45), 13987−13996.
(41) Oh, E.; Susumu, K.; Goswami, R.; Mattoussi, H. One-Phase Synthesis of Water-Soluble Gold Nanoparticles with Control over Size and Surface Functionalities. *Langmuir* **2010**, *26* (10), 7604−7613.
(42) Stewart, M. H.; Susumu, K.; Mei, B. C.; Medintz, I. L.; Delehanty, J. B.; Blanco-Canosa, J. B.; Dawson, P. E.; Mattoussi, H. Multidentate Poly(ethylene glycol) Ligands Provide Colloidal Stability to Semiconductor and Metallic Nanocrystals in Extreme Conditions. *J. Am. Chem. Soc.* **2010**, *132* (28), 9804−9813.
(43) Muhammed, M. A.; Aldeek, F.; Palui, G.; Trapiella-Alfonso, L.; Mattoussi, H. Growth of in situ functionalized luminescent silver nanoclusters by direct reduction and size focusing. *ACS Nano* **2012**, *6* (10), 8950−61.
(44) Aldeek, F.; Muhammed, M. A. H.; Palui, G.; Zhan, N. Q.; Mattoussi, H. Growth of Highly Fluorescent Polyethylene Glycol- and Zwitterion-Functionalized Gold Nanoclusters. *ACS Nano* **2013**, *7* (3), 2509−2521.
(45) Goulet, P. J. G.; Lennox, R. B. New Insights into Brust−Schiffrin Metal Nanoparticle Synthesis. *J. Am. Chem. Soc.* **2010**, *132* (28), 9582−9584.
(46) Mattoussi, H.; Mauro, J. M.; Goldman, E. R.; Anderson, G. P.; Sundar, V. C.; Mikulec, F. V.; Bawendi, M. G. Self-assembly of CdSe-ZnS quantum dot bioconjugates using an engineered recombinant protein. *J. Am. Chem. Soc.* **2000**, *122* (49), 12142−12150.
(47) Palui, G.; Avellini, T.; Zhan, N.; Pan, F.; Gray, D.; Alabugin, I.; Mattoussi, H. Photoinduced Phase Transfer of Luminescent Quantum

DOI: 10.1021/acs.langmuir.6b00950
Langmuir 2016, 32, 6445−6458

Dots to Polar and Aqueous Media. *J. Am. Chem. Soc.* **2012**, *134* (39), 16370−16378.
(48) Aldeek, F.; Hawkins, D.; Palomo, V.; Safi, M.; Palui, G.; Dawson, P. E.; Alabugin, I.; Mattoussi, H. UV and Sunlight Driven Photoligation of Quantum Dots: Understanding the Photochemical Transformation of the Ligands. *J. Am. Chem. Soc.* **2015**, *137* (7), 2704−2714.
(49) Huo, R.; Wehrens, R.; Buydens, L. M. C. Improved DOSY NMR data processing by data enhancement and combination of multivariate curve resolution with non-linear least square fitting. *J. Magn. Reson.* **2004**, *169* (2), 257−269.
(50) Susumu, K.; Mei, B. C.; Mattoussi, H. Multifunctional ligands based on dihydrolipoic acid and polyethylene glycol to promote biocompatibility of quantum dots. *Nat. Protoc.* **2009**, *4* (3), 424−436.
(51) Mei, B. C.; Susumu, K.; Medintz, I. L.; Mattoussi, H. Polyethylene glycol-based bidentate ligands to enhance quantum dot and gold nanoparticle stability in biological media. *Nat. Protoc.* **2009**, *4* (3), 412−423.
(52) Bucher, G.; Lu, C. Y.; Sander, W. The photochemistry of lipoic acid: Photoionization and observation of a triplet excited state of a disulfide. *ChemPhysChem* **2005**, *6* (12), 2607−2618.
(53) Stamplecoskie, K. G.; Chen, Y.-S.; Kamat, P. V. Excited-State Behavior of Luminescent Glutathione-Protected Gold Clusters. *J. Phys. Chem. C* **2014**, *118* (2), 1370−1376.
(54) Nirmal, M.; Murray, C. B.; Bawendi, M. G. Fluorescence-line narrowing in CdSe quantum dots: Surface localization of the photogenerated exciton. *Phys. Rev. B: Condens. Matter Mater. Phys.* **1994**, *50* (4), 2293−2300.
(55) Kasha, M. Characterization of electronic transitions in complex molecules. *Discuss. Faraday Soc.* **1950**, *9* (0), 14−19.
(56) Zhang, P.; Sham, T. K. X-Ray Studies of the Structure and Electronic Behavior of Alkanethiolate-Capped Gold Nanoparticles: The Interplay of Size and Surface Effects. *Phys. Rev. Lett.* **2003**, *90* (24), 245502.
(57) Tanaka, A.; Takeda, Y.; Imamura, M.; Sato, S. Dynamic final-state effect on the Au 4f core-level photoemission of dodecanethiolate-passivated Au nanoparticles on graphite substrates. *Phys. Rev. B: Condens. Matter Mater. Phys.* **2003**, *68*, 19.
(58) Salorinne, K.; Lahtinen, T.; Koivisto, J.; Kalenius, E.; Nissinen, M.; Pettersson, M.; Häkkinen, H. Nondestructive Size Determination of Thiol-Stabilized Gold Nanoclusters in Solution by Diffusion Ordered NMR Spectroscopy. *Anal. Chem.* **2013**, *85* (7), 3489−3492.
(59) Reichardt, C. Solvatochromic Dyes as Solvent Polarity Indicators. *Chem. Rev.* **1994**, *94* (8), 2319−2358.
(60) Leatherdale, C. A.; Bawendi, M. G. Observation of solvatochromism in CdSe colloidal quantum dots. *Phys. Rev. B: Condens. Matter Mater. Phys.* **2001**, *63* (16), 165315.

DOI: 10.1021/acs.langmuir.6b00950
Langmuir 2016, 32, 6445−6458